Computer Vision and Image Understanding 115 (2011) 1134–1144

Contents lists available at ScienceDirect

Computer Vision and Image Understanding

journal homepage: www.elsevier.com/locate/cviu

Color texture image segmentation based on neutrosophic set and wavelet transformation

Abdulkadir Sengur [a], Yanhui Guo [b,*]

[a] Department of Computer and Electronics Science, Firat University, 23119 Elazig, Turkey
[b] Department of Radiology, University of Michigan, Ann Arbor, MI 48109, USA

ARTICLE INFO

Article history:
Received 21 April 2010
Accepted 1 April 2011
Available online 15 April 2011

Keywords:
Neutrosophic set
Color texture image segmentation
Wavelet transform

ABSTRACT

Efficient and effective image segmentation is an important task in computer vision and pattern recognition. Since fully automatic image segmentation is usually very hard for natural images, interactive schemes with a few simple user inputs are good solutions. In this paper, we propose a fully automatic new approach for color texture image segmentation based on neutrosophic set (NS) and multiresolution wavelet transformation. It aims to segment the natural scene images, in which the color and texture of each region does not have uniform statistical characteristics. The proposed approach combines color information with the texture information on NS and wavelet domain for segmentation. At first, it transforms each color channel and the texture information of the input image into the NS domain independently. The entropy is defined and employed to evaluate the indeterminacy of the image in NS domain. Two operations, α-mean and β-enhancement operations are proposed to reduce the indeterminacy. Finally, the proposed method is employed to perform image segmentation using a γ-K-means clustering. The determination of the cluster number K is carried out with cluster validity analysis. Two different segmentation evaluation criterions were used to determine the segmentations quality. Experiments are conducted on a variety of images, and the results are compared with those new existing segmentation algorithm. The experimental results demonstrate that the proposed approach can segment the color images automatically and effectively.

1. Introduction

The task of image segmentation is to separate a given image into different regions with homogenous properties [1]. In a color texture segmentation algorithm, a label is assigned to each pixel based on its color properties and texture properties. Although significant works have focused on developing algorithms based on either color [1,2] or texture features [3,4] separately, the area of combined color and texture segmentation remains open and active. Natural scenes generally contain the combination of color and texture. Therefore, combining color and texture features would be of significant benefit in distinguishing regions having the same color but different textures, and vice versa.

In the past few decades, many methods have been proposed to segment the color image [1–12]. Most of them were based on two basic properties of the pixels in relation to their local neighborhood: discontinuity and similarity [1]. The approaches based on discontinuity partition an image by detecting isolated points, lines and edges, which were known as edge detection techniques [15–17]. A particular class of segmentation techniques is based on multiresolution analysis [7,10,12–14]. Such methods are typically based on multiresolution transformations. In general, small details are detected in higher resolution images, while larger objects are segmented in coarser images.

Kim and Kim [5,6] proposed a multiresolution wavelet-based watershed image segmentation technique, using markers and a region merging procedure to reduce over-segmentation. Jung and Scharcanski [7] used a combined image denoising/enhancement technique based on a redundant wavelet transform for segmentation. Ma and Manjunath [8,9] proposed the Edge Flow segmentation technique, which consists of computing and updating changes in color and texture in a pre-defined scale. Deng and Manjunath [11] proposed the JSEG method for multiscale segmentation of color and texture, based on color quantization and region growing. Wy et al. [12] proposed a multiscale wavelet-based directional image force as external force for snake segmentation. Comaniciu and Meer [2] used a kernel in the joint spatial-range domain to filter image pixels and a clustering method to retrieve segmented regions. Ozden and Polat [13] proposed a color image segmentation method based on low-level features including color, texture and spatial information. Chen et al. [14] proposed a color texture image segmentation algorithm based on wavelet transform and adaptive clustering algorithm.

* Corresponding author.
E-mail address: yanhui.guo@aggiemail.usu.edu (Y. Guo).

1077-3142/$ - see front matter © 2011 Elsevier Inc. All rights reserved.
doi:10.1016/j.cviu.2011.04.001

Arbelaez and Cohen [29] proposed an algorithm for constrained segmentation. The proposed method is a front propagation algorithm on the ultra-metric contour map that constructs Voronoi tessellations with respect to collections of subsets of the image domain. The algorithm is parameter-free, computationally efficient and robust. However, it needs to place the seed point inside each object of interest in the image by a human user.

Ning et al. [30] presented a new region merging based interactive image segmentation method. It needs to roughly indicate the location and region of the object and background by using strokes, which are called markers. Moreover, a novel maximal-similarity based region merging mechanism was proposed to guide the merging process with the help of markers. The method is efficient but the human user dependent.

Zhang et al. [31] proposed a novel region-based ACM for image segmentation which was implemented with a new level set method named Selective Binary and Gaussian Filtering Regularized Level Set (SBGFRLS) method. The SBGFRLS method reduces the expensive re-initialization of the traditional level set method to make it more efficient.

Although the above techniques present good results, several disadvantages of the reviewed methods still exist. For example, the mean-shift method requires a manual selection of spatial (hs) and color (hr) bandwidths, and optionally a minimum area parameter (M) for region merging. Moreover, it is important to notice that JSEG is intended to be an unsupervised segmentation method, meaning that it is free of user-defined parameter. On the other hand, some of the methods such as [7,13,14] need no parameter adjustment; they yield over-segmentation and under segmentation results.

Neutrosophic set (NS), was proposed by Florentin Smarandache as a new branch of philosophy dealing with the origin, nature and scope of neutralities, as well as their interactions with different ideational spectra [18]. In neutrosophy theory, every event has not only a certain degree of truth, but also a falsity degree and an indeterminacy degree that have to be considered independently from each other [18]. Thus, a theory, event, concept, or entity, {A} is considered with its opposite {Anti-A} and the neutrality {Neut-A}. {Neut-A} is neither {A} nor {Anti-A}. The {Neut-A} and {Anti-A} are referred to as {Non-A}. According to this theory, every idea {A} is neutralized and balanced by {Anti-A} and {Non-A} [18]. NS provides a powerful tool to deal with the indeterminacy. Guo and Cheng gave an example about reviewing paper to explain how the NS works and how better it is [24].

Nowadays, neutrosophic algebraic structures have been investigated [19], while the neutrosophic framework has found several practical applications in a variety of different fields, such as relational data base systems, semantic web services [18], financial dataset detection [19] and new economies growth and decline analysis [20]. In this paper, we propose a new approach for color texture image segmentation that is based on neutrosophic set (NS) and multiresolution wavelet decompositions. We combine color information with the low-level features of grayscale component of the texture. The proposed approach transforms both each color channel of the input image and the wavelet decomposition of the grayscale image into the NS domain independently which is described using three membership sets: T, I and F. The entropy in NS is defined and employed to evaluate the indeterminacy. Two operations, α-mean and β-enhancement operations are proposed to reduce the set indeterminacy. Finally, the proposed method is employed to perform image segmentation using a γ-means clustering. Experiments are conducted on a variety of images, and our results are compared with those new existing segmentation algorithm.

In the proposed method, it overcomes the drawback of the original NS based segmentation method, and NS is used to describe the indeterminacy in the color texture image. The experimental results demonstrate that the proposed approach can segment the color images automatically and effectively.

In summary, the novelties of this paper are the following:

- A fully automatic approach for color texture image segmentation based on neutrosophic set and multiresolution wavelet transformation that enables segment the color texture image without human inactivation.
- Adaptively selection on parameters in neutrosophic set that enables to reduce the indeterminacy according to the characteristic of the image.
- Cluster validity analysis to determination of the cluster number.

The rest of the paper is organized as follows. Section 2 briefly reviews the general introduction of neutrosophic set and operations. In Section 3, the proposed method is described in details. Section 4 describes the conducted experiments and presents experimental evidence, while concluding remarks are drawn in Section 5.

2. Neutrosphic set

Define T, I, and F as neutrosophic components to represent {A}, {Neut-A}, and {Anti-A}. Let T, I, and F are real standard or non-standard sets of $]^{-}0, 1^{+}[$ with $supT = t\_sup$, $infT = t\_inf$, $supI = i\_sup$, $infI = i\_inf$, $supF = f\_sup$, $infF = f\_inf$ and $n\_sup = t\_sup + i\_sup + f\_sup$, $n\_inf = t\_inf + i\_inf + f\_inf$ [18]. T, I, and F are not necessarily intervals, but may be any real sub-unitary subsets. They are set-valued vector functions or operations depending on known or unknown parameters and may be continuous or discrete. Moreover, T, I, and F may overlap or be converted from one to the other. An element $A(t, i, f)$ belongs to the set in the following way: it is t true ($t \in T$), i indeterminate ($i \in I$) and f false ($f \in F$), where t, i, and f are real numbers in the sets T, I, and F.

2.1. Neutrsophic image

Here, an image is transferred to neutrosophic domain. Thus, the neutrosophic image P_{NS} is characterized by three membership sets T, I, and F. A pixel in the neutrosophic domain can be represented as $P(t, i, f)$ which means the pixel is t% true, i% indeterminate and f% false, where t varies in T, i varies in I, and f varies in F, respectively. A pixel $P(i, j)$ in the image domain is transformed into the neutrosophic domain, $P_{NS}(i, j) = \{T(i, j), I(i, j), F(i, j)\}$. $T(i, j)$, $I(i, j)$ and $F(i, j)$ are the membership value belonging to true set, indeterminate set and false set, respectively.

$$T(i,j) = \frac{\bar{g}(i,j) - \bar{g}_{\min}}{\bar{g}_{\max} - \bar{g}_{\min}} \tag{1}$$

$$\bar{g}(i,j) = \frac{1}{w \times w} \sum_{m=i-w/2}^{i+w/2} \sum_{n=j-w/2}^{j+w/2} g(m,n) \tag{2}$$

$$I(i,j) = \frac{\delta(i,j) - \delta_{\min}}{\delta_{\max} - \delta_{\min}} \tag{3}$$

$$\delta(i,j) = abs(g(i,j) - \bar{g}(i,j)) \tag{4}$$

$$F(i,j) = 1 - T(i,j) \tag{5}$$

where $\bar{g}(i, j)$ is the local mean value of the image. $\delta(i, j)$ is the absolute value of the difference between intensity $g(i, j)$ and its local mean value $\bar{g}(i, j)$ at (i, j).

For a gray level image, the entropy evaluates the distribution of the distribution of gray levels. If the entropy is big, the intensities

have equal probability and they distribute uniformly. If the entropy is small, the intensities have different probabilities and their distributions are non-uniform.

An entropy in neutrosphic image is defined as the summation of the entropies of three sets T, I and F, which is employed to evaluate the distribution of the elements in the neutrosphic domain:

$$En_{NS} = En_T + En_I + En_F \tag{6}$$

$$En_T = -\sum_{i=\min\{T\}}^{\max\{T\}} p_T(i)\ln p_T(i) \tag{7}$$

$$En_I = -\sum_{i=\min\{I\}}^{\max\{I\}} p_I(i)\ln p_I(i) \tag{8}$$

$$En_F = -\sum_{i=\min\{F\}}^{\max\{F\}} p_F(i)\ln p_F(i) \tag{9}$$

where En_T, En_I and En_F are the entropies of the sets T, I and F, respectively. $p_T(i)$, $p_I(i)$ and $p_F(i)$ are the probability of element i in T, I and F, respectively.

The value of $I(i,j)$ is employed to measure the indeterminacy degree of element $P_{NS}(i,j)$. For making T and F correlated with I, the changes in T and F influence the distribution of element in I and the entropy of I.

Two operations, α-mean operation and β-enhancement operation, are employed to decrease the indeterminacy in NS image.

An α-mean operation $\overline{P}_{NS}(\alpha)$ is defined to compute the mean value between the neighbors in NS:

$$\overline{P}_{NS}(\alpha) = P(\overline{T}(\alpha), \overline{I}(\alpha), \overline{F}(\alpha)) \tag{10}$$

$$\overline{T}(\alpha) = \begin{cases} T & I < \alpha \\ \overline{T}_\alpha & I \geqslant \alpha \end{cases} \tag{11}$$

$$\overline{T}_\alpha(i,j) = \frac{1}{w\times w}\sum_{m=i-w/2}^{i+w/2}\sum_{n=j-w/2}^{j+w/2} T(m,n) \tag{12}$$

$$\overline{F}(\alpha) = \begin{cases} F & I < \alpha \\ \overline{F} & I \geqslant \alpha \end{cases} \tag{13}$$

$$\overline{F}_\alpha(i,j) = \frac{1}{w\times w}\sum_{m=i-w/2}^{i+w/2}\sum_{n=j-w/2}^{j+w/2} F(m,n) \tag{14}$$

$$\overline{I}_\alpha(i,j) = \frac{\bar{\delta}_T(i,j) - \bar{\delta}_{T\min}}{\bar{\delta}_{T\max} - \bar{\delta}_{T\min}} \tag{15}$$

$$\bar{\delta}_T(i,j) = abs(\overline{T}(i,j) - \overline{\overline{T}}(i,j)) \tag{16}$$

$$\overline{\overline{T}}(i,j) = \frac{1}{w\times w}\sum_{m=i-w/2}^{i+w/2}\sum_{n=j-w/2}^{j+w/2} \overline{T}(m,n) \tag{17}$$

where $\bar{\delta}_T(i,j)$ is the absolute value of the difference between the mean intensity $\overline{T}(i,j)$ and its mean value $\overline{\overline{T}}(i,j)$ after the α-mean operation.

In NS, an enhancement operation, β-enhancement operation, $P'_{NS}(\beta)$, is defined as:

$$P'_{NS}(\beta) = P(T'(\beta), \quad I'(\beta), \quad F'(\beta)) \tag{18}$$

$$T'(\beta) = \begin{cases} T & I < \beta \\ T'_\lambda & I \geqslant \beta \end{cases} \tag{19}$$

$$T'_\beta(i,j) = \begin{cases} 2T^2(i,j) & T(i,j) \leqslant 0.5 \\ 1 - 2(1 - T(i,j))^2 & T(i,j) > 0.5 \end{cases} \tag{20}$$

$$F'(\beta) = \begin{cases} F & I < \beta \\ F'_\lambda & I \geqslant \beta \end{cases} \tag{21}$$

$$F'_\beta(i,j) = \begin{cases} 2F^2(i,j) & F(i,j) \leqslant 0.5 \\ 1 - 2(1 - F(i,j))^2 & F(i,j) > 0.5 \end{cases} \tag{22}$$

$$I'_\beta(i,j) = \frac{\delta'_T(i,j) - \delta'_{T\min}}{\delta'_{T\max} - \delta'_{T\min}} \tag{23}$$

$$\delta'_T(i,j) = abs(T'(i,j) - \overline{T}'(i,j)) \tag{24}$$

$$\overline{T}'(i,j) = \frac{1}{w\times w}\sum_{m=i-w/2}^{i+w/2}\sum_{n=j-w/2}^{j+w/2} T'(m,n) \tag{25}$$

where $\delta'_T(i,j)$ is the absolute value of difference between intensity $T'(i,j)$ and its local mean value $\overline{T}'(i,j)$ at (i,j) after the β-enhancement operation. After the β-enhancement operation, the membership set T becomes more distinct and has high contrast, which is suitable for segmentation.

In [24], two important parameters α and β were selected as a constant value: 0.85, which affect the segmentation results. If α and β are not appropriate, the method will fail into worse results. Fig. 1 is an example to show the drawback of α and β parameters selection in NS segmentation approach. This image is corrupted with the Gaussian noise, whose mean is 0 and variance is 31.365. When α and β are both 0.85, the segmentation result is shown in Fig. 1b. If $\alpha = 0.25$ and $\beta = 0.95$, that these values are obtained using Eqs. (26)–(29), we can obtain more consistent and homogenous re-

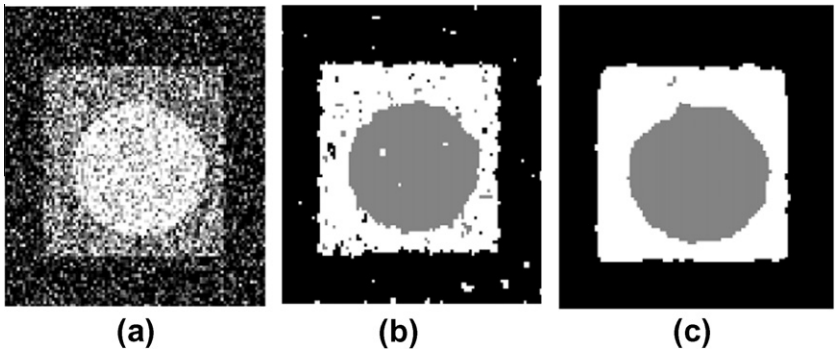

Fig. 1. (a) Original image with Gaussian noise, (b) NS segmentation result with $\alpha = 0.85$ and $\beta = 0.85$, (c) NS segmentation result with $\alpha = 0.25$ and $\beta = 0.95$.

gions depicted in Fig. 1c. So, the values of α and β should be selected based on the image's characteristic.

In this paper, in order to overcome the drawback of the original NS based segmentation method; we determine the parameters adaptively according to the characteristic of the processed images. The parameters of α and β are computed as:

$$EnI = -\sum_{i=1}^{h}\sum_{j=1}^{w} p(i,j)\log_2 p(i,j) \tag{26}$$

$$En_{\max} = -\log_2 \frac{1}{hw} \tag{27}$$

$$\alpha = \alpha_{\min} + \frac{(\alpha_{\max} - \alpha_{\min})(EnI - En_{\min})}{(En_{\max} - En_{\min})} \tag{28}$$

$$\beta = 1 - \alpha \tag{29}$$

where h and w are the height and width of the image. Here, $En_{\min} = 0$, $\alpha_{\min} = 0.01$ and $\alpha_{\max} = 0.1$ are determined by our experiments. The parameter β is used to reduce the indeterminacy. We employed an entropy measurement to evaluate the change of the local pixels. When the entropy is high, the indeterminacy is high and the value of β should be small.

A new clustering method is defined in NS and it deals with $\overline{P}_{NS}(\alpha,\beta)$ after the α-mean and β-enhancement operations in NS domain. Considering the effect of indeterminacy, we composed the two set, T and I into a new set for clustering.

$$X(i,j) = \begin{cases} T(i,j) & I(i,j) \leqslant \gamma \\ \overline{T}_{\gamma}(i,j) & I(i,j) > \gamma \end{cases} \tag{30}$$

The new K-means cluster for the neutrosophic set, γ-K-means, is applied to the subset T. The new objective function of γ-means is defined as:

$$J_{TC} = \sum_{l=1}^{K}\sum_{i=1}^{H}\sum_{j=1}^{W} \|X(i,j) - Z_l\|^2 \tag{31}$$

$$Z_l = \frac{1}{n_l}\sum_{X(ij)\in C_l} X(i,j) \tag{32}$$

Moreover, we adapted the validity index of Xie and Beni [32] to neutrosophic domain to obtain the number of clusters K automatically. The adaptation is as following;

$$N_{XB}(K) = \frac{J_{TC}}{n.\min_{ij}||Z_i - Z_j||^2} \tag{33}$$

where J_{TC} is a compactness measure, n is the number of data to be clustered and the denominator of N_{XB} is a separation measure. In general, an optimal K^* is found by solving $\min_{2\leqslant K\leqslant n-1} N_{XB}(K)$ to produce a best clustering performance for the data set X.

3. The proposed method

Neutrosophic set had been applied to image thresholding, image denoise and image segmentation applications [22–24]. Cheng and Guo [22] proposed a thresholding algorithm based on neutrosophy, which could select the thresholds automatically and effectively. In [23], some concepts and operators were defined based on NS and applied for image denoising. It can process not only noisy images with different levels of noise, but also images with different kinds of noise well. NS for image segmentation were also studied in [24].

As we declared in previous section, two of the basic approaches for image segmentation are region and boundary based. The literature for the last decade is full of a large set of proposals which attempt to segment the image based on one of these approaches. However, based on the complementary nature of the edge and region information, current trends on image segmentation are to integrate both sources to obtain better results. There are also two basic properties that can be considered for grouping pixels and define the concept of similarity: color and texture. The importance of both features in order to define the visual perception is obvious in images corresponding to natural scenes which have considerable variety of color and texture. However, most of the literature deals with segmentation based on either color or texture and few proposals consider both properties together.

In this paper, we propose a novel color texture image segmentation algorithm based on wavelet transform and neutrosophic sets. In the first step, the $L*u*v$ color components and the gray scale image are obtained from the RGB color texture input image. Then, wavelet transform is applied to gray scale image to obtain the LL, LH, HL, and HH sub-bands. Only, LH and HL sub-bands are employed for further processes because most of the texture information is in the LH and HL sub-bands. We then calculate the mean energy using coefficients of LH and HL sub-bands in a local window. The energy is defined as the square of the coefficients, and used for texture characterization. The pixel $P(i,j)$ in the image domain for each L, u and v channels and the energy component in wavelet domain is transformed into the neutrosophic domain using Eqs. (1)–(5). The indeterminacy of the NS image P_{NS} is decreased by using the α-mean and β-enhancement operations on subset T of each L, u and v channels and energy component of wavelet domain according to Eqs. (10)–(25). The values of α and β parameters are determined automatically using Eqs. (26)–(29). The elements in subset T for each color channel and energy component of wavelet domain are combined as the input for the γ-K-means clustering. The clustering process is employed and objective function is defined according to Eqs. (30)–(32).

The segmentation algorithm is summarized as below:

Step 1: Convert image from RGB color space to $L*u*v$ color space and decompose each color channel L, u and v.
Step 2: Obtain gray scale image from RGB color space.
Step 3: Use wavelet transformation to decompose the gray scale image into sub-bands (LL, LH, HL, and HH).
Step 4: Calculate the mean energies of LH and HL sub-bands, $MELH$ and $MEHL$.

$$MELH(i,j) = \frac{1}{wxw}\sum_{k=-w/2}^{w/2}\sum_{l=-w/2}^{w/2} LH(i+k,j+l) \tag{34}$$

$$MEHL(i,j) = \frac{1}{wxw}\sum_{k=-w/2}^{w/2}\sum_{l=-w/2}^{w/2} HL(i+k,j+l) \tag{35}$$

where w is the size of the sliding window.

Step 5: Transform the L, u and v color channels and wavelet mean energy sub-bands into NS domain independently using Eqs. (1)–(5), which are represented as L_{NS}, u_{NS}, v_{NS}, $MELH_{NS}$, and $MEHL_{NS}$;
Step 6: Obtain α and β parameters using Eqs. (26)–(29) and perform the α-mean and-β-enhancement operations on the true subsets of L_{NS}, u_{NS}, v_{NS}, $MELH_{NS}$, and $MEHL_{NS}$;
Step 7: Compute the entropy of the indeterminate subset, EnI(i) of L_{NS}, v_{NS}, v_{NS}, $MELH_{NS}$, and $MEHL_{NS}$, respectively;
Step 8: If EnI(i + 1)-EnI(i)/EnI(i) < ξ, goto Step 9; else go to Step 6;
Step 9: Apply the γ-K-means clustering to the true subset. The input of the clustering algorithm is a vector $X = [T_{L_{NS}}, T_{u_{NS}},$

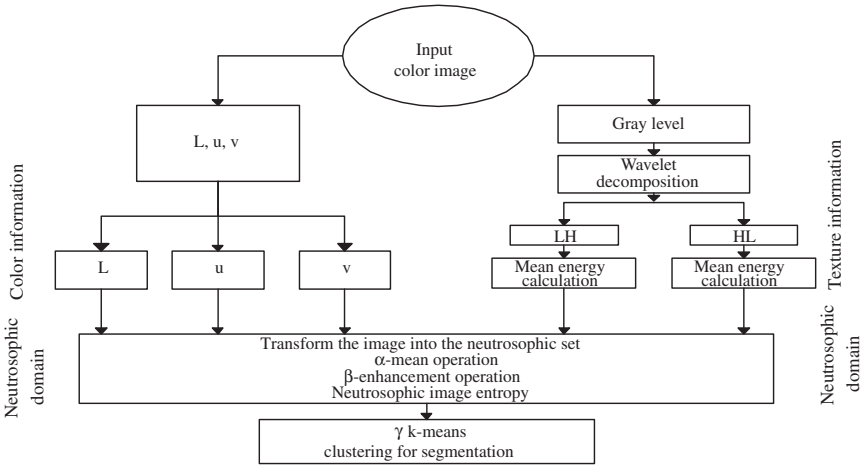

Fig. 2. The flowchart of the color texture image segmentation algorithm.

$T_{v_{NS}}, T_{MELH_{NS}}, T_{MEHL_{NS}}]$, which combine the true subsets of L_{NS}, v_{NS}, v_{NS}, $MELH_{NS}$, and $MEHL_{NS}$;

Step 10: Segment the image according to the result in Step 9.

The flowchart of the proposed algorithm is shown in Fig. 2.

4. Experiments and discussion

In the experiments, we use the 2/2 biorthogonal wavelet decomposition [21], which is separable and computationally efficient. We obtain the one-level wavelet decomposition, and use the HL and LH bands, where H and L stand for the high-pass and low-pass band in each of the horizontal and vertical orientations. We found that discarding the HH band does not result in any significant loss of visual quality, and hence it should not be critical for texture analysis.

The most commonly used feature for texture analysis in the wavelet domain is the energy of the sub-band coefficients [14]. Since the coefficients are quite sparse, it is necessary to perform some type of window operation to obtain a more uniform characterization of texture. In this paper, we use the mean of the energy in a window. The size of the window must be large enough to capture the local texture characteristics, but not too large to avoid border effects. We found that for the image resolution and viewing distance under consideration, a 5×5 window gives the best results.

Firstly, we compared the performance of the proposed approach with that of the original NS based method [24]. The NS based method is quite well for gray level image segmentation but its ability to segment the color texture image is limited. We experimented on several natural color texture images and the results can be seen in Fig. 3. The original images are given in the first column, ground-truth segmentations are given in the second column, proposed

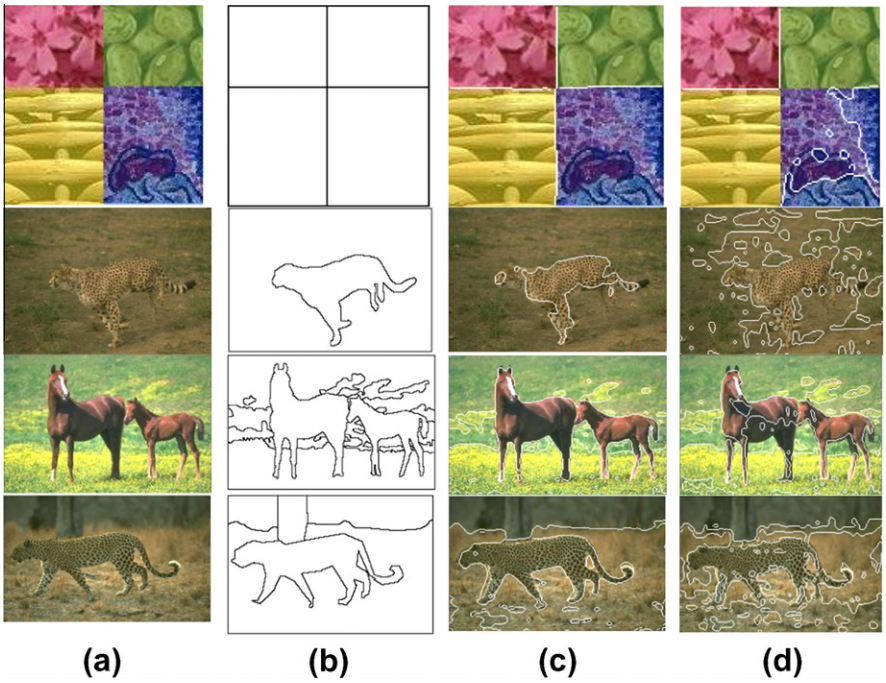

Fig. 3. (a) Original image. (b) Ground-truth segmentation. (c) Results by the proposed method. (d) Results by [24].

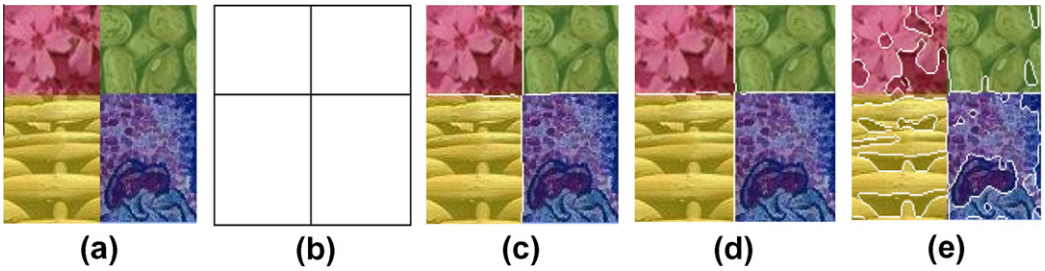

Fig. 4. (a) Original texture image. (b) Ground-truth segmentation result. (c) Image segmentation results using proposed approach. (d) MSF-HDS [13]. (e) Waveseg [10].

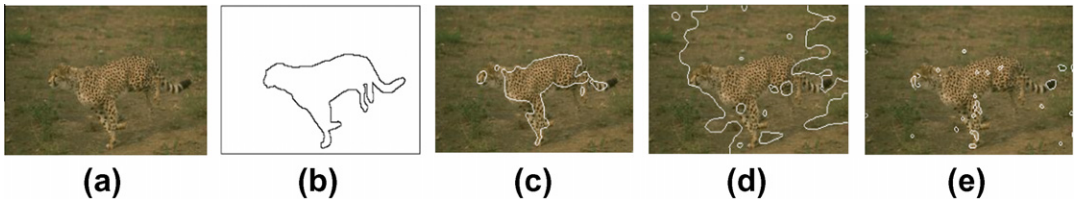

Fig. 5. (a) Cheetah image. (b) Ground-truth segmentation result. (c) Image segmentation results using proposed approach. (d) MSF-HDS [13]. (e) Waveseg [10].

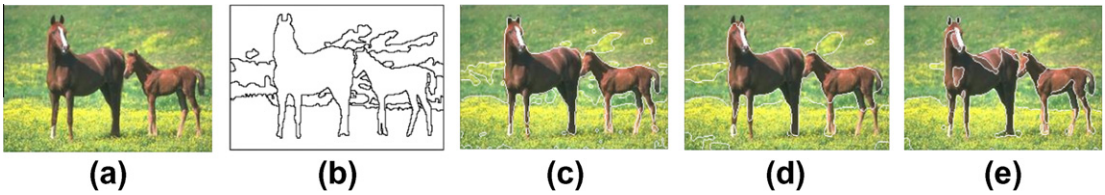

Fig. 6. (a) 'Horse' image. (b) Ground-truth segmentation result. (c) Image segmentation results using proposed approach. (d) MSF-HDS [13]. (e) Waveseg [10].

Table 1
FOM results for our proposal, MSF-HDS and Waveseg.

Image	Our proposal	MSF-HDS	Waveseg
Fig. 4	0.8144	0.8138	0.1824
Fig. 5	0.3921	0.1811	0.1738
Fig. 6	0.4572	0.3341	0.3767

Table 2
F-measure for the comparison between the proposed method, MSF-HDS and Waveseg.

Image	Our proposal	MSF-HDS	Waveseg
Fig. 4	0.9319	0.9201	0.4401
Fig. 5	0.6937	0.4194	0.2176
Fig. 6	0.8385	0.7390	0.5433

Table 3
FOM results for our proposal, MSF-HDS and Waveseg.

Image	Our proposal	MSF-HDS	Waveseg
Fig. 7	0.4404	0.2533	0.2855

Table 4
F-measure for the comparison between the proposed method, MSF-HDS and Waveseg.

Image	Our proposal	MSF-HDS	Waveseg
Fig. 7	0.6850	0.4721	0.2805

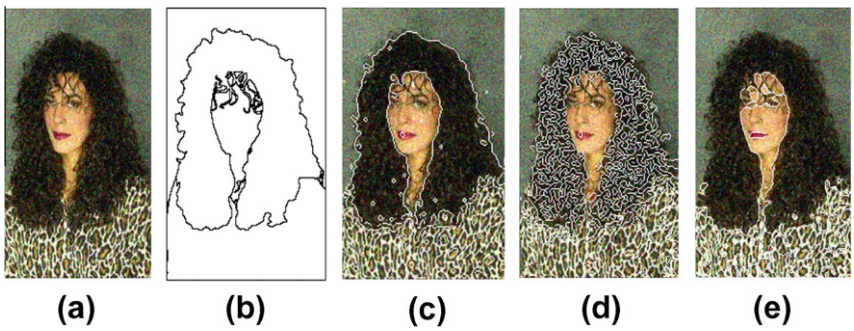

Fig. 7. (a) Noisy 'Woman' image. (b) Ground-truth segmentation result. (c) Image segmentation results using proposed approach. (d) MSF-HDS [13]. (e) Waveseg [10].

Fig. 8. (a) Image segmentation results using proposed approach. (b) Ground-truth segmentation result. (c) MSF-HDS [13]. (d) Waveseg [10].

method's segmentation results are given in the third column and the original NS based method's segmentation results are given in the fourth column of Fig. 3, respectively. The first experiment is carried out on a texture image that is given in first row of Fig. 3. This color texture image is composed of four regions. Thus, the number of clusters K is 4 for γ-K-means clustering. Our proposal al-

Fig. 8 (*continued*)

most obtained 100% correct segmentation when we consider the ground-truth image. The boundaries of the each segment located smoothly. On the other hand, NS based method could not segment the texture image accordingly. Only the pink texture region is correctly segmented. The other regions are wrongly segmented. Moreover, the dark blue region is over-segmented. The boundaries are not located correctly.

A 'Cheetah' image is used in the second experiment. This image can be divided into two main parts; Cheetah and background. Subsequently, the K value of the γ-K-means clustering is 2. A considerably worse segmentation is obtained by NS based method. Cheetah and background regions are not separated. On the other hand, our proposal obtained a better segmentation than NS based method. The background is correctly separated. Only few parts of the Cheetah are wrongly segmented. When we consider the rest experiments, similar successful segmentation results, which are obtained by our proposal, can be seen in the third and fourth row of the Fig. 3. The horses and the tiger are correctly segmented. Several background regions are wrongly segmented. But the boundaries of the objects are correctly located. However, NS based method again produced worse segmentation results. The objects regions are not homogenous. The boundaries are not smooth and the some of the boundaries are wrongly located on the objects.

Moreover, we have applied the proposed approach to a variety of images and also compared it with two state-of-the-art segmentation methods, namely, mean shift filtering in higher dimensional space (MSF-HDS) [13] and Waveseg [10]. For MSF-HDS, we used the parameters h_s, h_r and M following the guidelines provided in [13]. In Waveseg [10] method, the segmentation procedure is controlled with two parameters, namely scale parameter J and region merging threshold T_c. We used default values as described in [10].

There is no a universally accepted objective criterion to evaluate the performance of the color image segmentation algorithms yet. However, we can know the desired results that are constructed by ground truth or human-segmented image, and we can use some objective criteria to evaluate the algorithms. The approach adopted here is to use the ground truth provided by a simulated image in conjunction with the most widely used measure of edge deviation, Pratt's figure of merit (FOM) [25]. Pratt considered three major areas of error associated with the determination of an edge: missing valid edge points; failure to localize edge points; classification of noise fluctuations as edge points. In addition to these consider-

ations, when measuring edge detection performance, edge detectors that produce smeared edge locations should be penalized, whilst those that produce edge locations that are localized should be awarded credit. Hence Pratt introduced the FOM technique as one that balances the three types of error above, defined as;

$$FOM = \frac{1}{\max\{I_D, I_I\}} \sum_{k=1}^{I_D} \frac{1}{1 + \alpha(d_k)^2} \tag{36}$$

where I_I and I_D are the number of ideal and detected edge points, respectively, and d_k is the separation distance of the kth detected edge point normal to a line of ideal edge points. The scaling constant $\alpha > 0$ provides a relative penalty between smeared and isolated, offset edges and was set to $\alpha = 1/9$. A FOM = 1 corresponds to a perfect match between the ideal and detected edge points and as the deviation of the detected points increases, the FOM approaches zero.

We also used another criterion, called *F*-measure, to measure the goodness of our proposal and the other methods (MSF-HDS and Waveseg) that we have used for comparison purposes. In [28], a way to match segmentation to the ground truth and calculating precision and recall for the match is proposed. Thinned edges are matched to the ground truth and based on this match; precision (P) and recall (R) are calculated. To define a single goodness measure from precision and recall, the *F*-measure has been used:

$$F = \frac{P \cdot R}{\xi \cdot P + (1 - \xi) \cdot R} \tag{37}$$

where ξ defines the tradeoff between precision and recall. In [28], ξ is selected as 0.5, which we also follow.

To demonstrate the performance of the algorithms, we experimented with a number of natural images. The texture image was taken from the MIT VisTex database (http://vismod.media.mit.edu/vismod/imagery/VisionTexture/vistex.html) [26]. An image in Fig. 4 is employed to illustrate the performance of the proposed algorithm. The image contains four distinct classes. The ground-truth segmentation image was obtained manually. The proposed NS based color image segmentation approach was implemented in MATLAB and MSF-HDS and Waveseg results were obtained using MATLAB implementations provided by the authors.

We applied our proposal, MSF-HDS and Waveseg algorithm to the original image which is depicted in Fig. 4a and the corresponding results are given in Fig. 4c, d and e, respectively. Our proposal and MSF-HDS produced similar results that are depicted in Fig. 4c and d, respectively, for the original image. These results almost match the ground-truth image that is depicted in Fig. 4b. These results are also better than the Waveseg outcome. Waveseg could not produce the correct boundaries of the different regions. There is over-segmentation in all four regions of the image.

A 'Cheetah' image which was taken from the web site of http://www.eecs.berkeley.edu/Research/Projects/CS/vision is used for comparison purposes [27]. The pixels of the 'Cheetah' image of Fig. 5a can be divided into two main classes, namely the background and the Cheetah. Our proposal yielded better segmentation than other methods (Fig. 5c). Although, the whole cheetah is not correctly segmented, when we consider the ground-truth segmentation image in Fig. 5b, the obtained segmentation is considerably successful. The background region is obtained clearly. Fig. 5d shows the MSF-HDS result for the original image. No Cheetah region is found. Moreover, some of the background region is labeled as Cheetah. Unfortunately, Waveseg produced the worst segmentation result as can be seen in Fig. 5e. Almost whole image is labeled as background. Only small holes are labeled as Cheetah.

A 'Horse' image which was taken from the web site of http://www.eecs.berkeley.edu/Research/Projects/CS/vision is given in Fig. 6. This image can be divided into three classes, namely grass, horses and yellow flowers region. There are also yellow flower regions in the grass region. At the first sight, it could be seen that our proposal and MSF-HDS produced almost the same segmentation results. But, when the results of both methods examine carefully, the superiority of our proposal can be realized. The ears of the big horse could not be segmented by the MSF-HDS method. In addition, one leg of the baby horse was also missed by the MSF-HDS. Moreover, the yellow flower regions in the grass area were not segmented in detailed. On the other hand, our proposal result in Fig. 6c is more homogenous and the boundaries are smoother. The yellow flowers regions in the grass area were segmented. The worse result is produced by Waveseg. There are over-segmentation area in the horse regions. The yellow regions in the grass are also missed.

In Table 1, the FOM values are given to indicate the quality of the segmentations results by the three methods. According to the FOM results, it is indicated one more times that our proposal yielded better segmentation results than MSF-HDS and Waveseg.

Moreover, the *F*-measure results are shown in Table 2. The proposed approach produces segmentations of high quality and with better results than the other methods for all tested images.

We also evaluated our segmentation method on noisy images. An example of noisy image is given in Fig. 7a. This 'woman' image can be divided into four classes, namely background, hair, face and blouse region. This 'woman' image was corrupted by Gaussian noise, whose mean is 0 and variance is 0.01 and the related segmentation results are given in Fig. 7c, d and e, respectively.

Although the 'Woman' image was corrupted with Gaussian noise, our proposal almost produced a ground-truth segmentation result that is given in Fig. 7b. Although there are only several misclassified small regions in the hair and blouse regions, the boundaries of the segmentation are smooth and almost fitted on the ground-truth segmentation. On the other hand, MSF-HDS did not produce a successful segmentation (Fig. 7d). There are both over-

Table 5
FOM results of natural images for our proposal, MSF-HDS and Waveseg.

Image	Our proposal	MSF-HDS	Waveseg
Fig. 8 (1)	0.4740	0.4071	0.2864
Fig. 8 (2)	0.6352	0.5632	0.6237
Fig. 8 (3)	0.4790	0.3249	0.3273
Fig. 8 (4)	0.5514	0.4809	0.4494
Fig. 8 (5)	0.4976	0.2003	0.5896
Fig. 8 (6)	0.4453	0.3334	0.3720
Fig. 8 (7)	0.4134	0.3774	0.3339
Fig. 8 (8)	0.5974	0.5714	0.5619
Fig. 8 (9)	0.6398	0.4243	0.5776
Fig. 8 (10)	0.4649	0.3823	0.3051
Fig. 8 (11)	0.5821	0.5274	0.3971

Table 6
F-measure values of natural images for our proposal, MSF-HDS and Waveseg.

Image	Our proposal	MSF-HDS	Waveseg
Fig. 8 (1)	0.7267	0.5812	0.3817
Fig. 8 (2)	0.9421	0.9109	0.9354
Fig. 8 (3)	0.7634	0.5564	0.3126
Fig. 8 (4)	0.8974	0.8438	0.7989
Fig. 8 (5)	0.8196	0.6782	0.8246
Fig. 8 (6)	0.7478	0.6390	0.5178
Fig. 8 (7)	0.6128	0.5818	0.3354
Fig. 8 (8)	0.9126	0.8987	0.7612
Fig. 8 (9)	0.8817	0.8542	0.7890
Fig. 8 (10)	0.8896	0.7610	0.6134
Fig. 8 (11)	0.8288	0.7921	0.6739

Table 7
The $N_{XB}(K)$ and F-measure values for cluster number $K = 2, 3, \ldots, 9$.

	K	2	3	4	5	6	7	8	9
Fig. 4	$N_{XB}(K)$	0.1772	0.1697	0.1081	0.2107	0.8575	0.6287	0.4129	0.3006
	F-measure	0.6529	0.7641	0.9319	0.5400	0.4683	0.3971	0.3616	0.3803
Fig. 5	$N_{XB}(K)$	0.1085	0.4858	0.8041	0.5815	0.9114	0.7360	0.5971	0.9179
	F-measure	0.6937	0.3165	0.2882	0.2793	0.2739	0.2569	0.2624	0.2525
Fig. 6	$N_{XB}(K)$	0.1079	0.0680	0.0918	0.0980	0.0998	0.0861	0.1006	0.1234
	F-measure	0.6776	0.8385	0.8115	0.7925	0.8087	0.7724	0.7773	0.7590

segmentation and misclassified pixels. The hair of the woman is labeled as two different classes. The blouse of the woman is also over-segmented. The region boundaries of the woman image did not located correctly. Waveseg method also produced bad segmentation results (Fig. 7e). But, it yielded better result than MSF-HDS.

In Tables 3 and 4, the FOM and the F-measure values were also calculated to indicate the quality of the segmentation results of a noisy image by the three methods, respectively. According to the FOM and F-measure results, it is indicated one more times that our proposal yielded better segmentation results than MSF-HDS and Waveseg.

We also applied our technique to several natural images contained in the Berkeley dataset, and compared results with MSF-HDS and Waveseg segmentation algorithm and manual delineations provided with the database (darker contours were marked by more human subjects) [25]. An overall visual inspection indicates that our proposal produced better segmentation results as shown in Fig. 8. The FOM and the F-measure values for each image indicate our proposal success. These results can be seen in Tables 5 and 6.

Finally, we did several experiments to present the sensitivity of the proposed segmentation method with respect to cluster number K. We implemented the sensitivity analysis experimentations in Figs. 4–6 images with the cluster number $K = 2, 3, \ldots, 9$. The $N_{XB}(K)$ and F-measure values were calculated for each image with the cluster number K and the calculated values were listed in Table 7. The Fig. 4 has four distinct regions. The minimum $N_{XB}(K)$ value was achieved when the cluster number is 4. Moreover, according to the F-measure, the best segmentation result was obtained when the cluster number is also 4. On the other hand, the segmentation results are considerably poor for other cluster numbers.

In Fig. 5, there is a running cheetah. By visual inspection, there are only two regions: cheetah and background. So, the expected cluster number is 2. The related values from Table 7 for Fig. 5 verify our inspection. The minimum $N_{XB}(K)$ and maximum F-measure values were obtained while the cluster number was 2.

Fig. 6 contains three regions, e.g., horses and two different grass-textured regions. One more time, calculated $N_{XB}(K)$ and F-measure values indicated the true cluster number.

5. Conclusions

In this paper, we proposed a wavelet domain NS for color texture image segmentation. The NS domain operations are applied to both color channels and the wavelet domain features of the input color texture image simultaneously. The color texture image is converted to gray scale image by linear transformation to obtain the textural features. One-level wavelet decomposition is applied to grayscale image and the mean of the energy is calculated in a window on the wavelet coefficients. The size of the window must be large enough to capture the local texture characteristics. After NS domain process, all color and texture features are combined for γ-K-means clustering. We have applied the proposed approach to a variety of images and compared the performance with MSF-HDS and Waveseg. The segmentation result using proposed algorithm is better than MSF-HDS and Waveseg method.

References

[1] H.D. Cheng, X.H. Jiang, Y. Sun, J.L. Wang, Color image segmentation: advances and prospects, Pattern Recognition 34 (12) (2001) 2259–2281.
[2] D. Comanicui, P. Meer, Mean shift: a robust approach toward feature space analysis, IEEE Transactions on Pattern Analysis and Machine Intelligence 24 (5) (2002).
[3] A. Sengur, İ Türkoğlu, M.C. İnce, Wavelet oscillator neural networks for texture segmentation, Neural Network World 4 (2008) 275–289.
[4] A. Sengur, Wavelet transform and adaptive neuro-fuzzy inference system for color texture classification, Expert Systems with Applications 34 (3) (2008) 2120–2128.
[5] J.B. Kim, H.J. Kim, A wavelet-based watershed image segmentation for VOP generation, IEEE International Conference on Pattern Recognition (2002) 505–508.
[6] J.B. Kim, H.J. Kim, Multiresolution-based watersheds for efficient image segmentation, Pattern Recognition Letters 24 (2003) 473–488.
[7] C. Jung, J. Scharcanski, Robust watershed segmentation using wavelets, Image and Vision Computing 23 (7) (2005) 661–669.
[8] W.Y. Ma, B.S. Manjunath, Edge flow: a framework of boundary detection and image segmentation, IEEE Conference on Computer Vision and Pattern Recognition 9 (1997) 744–749.
[9] W.Y. Ma, B.S. Manjunath, Edge flow: a technique for boundary detection and image segmentation, IEEE Transactions on Image Processing 9 (8) (2000) 1375–1388.
[10] C.R. Jung, Unsupervised multiscale segmentation of color images, Pattern Recognition Letters 28 (2007) 523–533.
[11] Y. Deng, B.S. Manjunath, Unsupervised segmentation of color-texture regions in images and video, IEEE Transactions on Pattern Analysis and Machine Intelligence 23 (8) (2001) 800–810.
[12] H. Wu, J. Liu, C. Chui, A wavelet-frame based image force model for active contouring algorithms, IEEE Transactions on Image Processing 9 (11) (2000) 1983–1987.
[13] M. Ozden, E. Polat, A color image segmentation approach for content-based image retrieval, Pattern Recognition 40 (2007) 1318–1325.
[14] J. Chen, T.N. Pappas, A. Mojsilovic, B. Rogowitz, Image segmentation by spatially adaptive color and texture features, in: Proceedings of IEEE International Conference on Image Processing (ICIP'03), Barcelona, Spain, September 2003.
[15] M. Maire, P. Arbelaez, C. Fowlkes, J. Malik, Using contours to detect and localize junctions in natural images, IEEE Conference on Computer Vision and Pattern Recognition (2008) 1–8.
[16] Xiaofeng Ren, Multi-scale improves boundary detection in natural images, ECCV, 2008.
[17] Piotr Dollar, Zhuowen Tu, Serge Belongie, Supervised learning of edges and object boundaries, IEEE Computer Vision and Pattern Recognition (CVPR), June 2006.
[18] F. Smarandache, A Unifying Field in Logics Neutrosophic Logic. Neutrosophy, Neutrosophic Set, Neutrosophic Probability, third ed., American Research Press, 2003.
[19] H. Wang, R. Sunderraman, F. Smarandache, Y.Q. Zhang, Interval neutrosophic sets and logic: theory and applications in computing, Infinite Study (2005).
[20] M. Khoshnevisan, S. Singh, Neurofuzzy and neutrosophic approach to compute the rate of change in new economies, in: F. Smarandache (Ed.), Proceedings of the First International Conference on Neutrosophy, Neutrosophic Logic, Neutrosophic Set, Neutrosophic Probability and Statistics, University of New Mexico, 2002, pp. 56–62.
[21] A. Cohen, I. Daubechies, J.C. Feauveau, Biorthogonal bases of compactly supported wavelets, Communications on Pure and Applied Mathematics 45 (1992) 485–560.
[22] H.D. Cheng, Y. Guo, A new neutrosophic approach to image thresholding, New Mathematics and Natural Computation 4 (3) (2008) 291–308.
[23] Y. Guo, H.D. Cheng, A new neutrosophic approach to image denoising, New Mathematics and Natural Computation 5 (3) (2009) 653–662.
[24] Y. Guo, H.D. Cheng, A new neutrosophic approach to image segmentation, Pattern Recognition 42 (2009) 587–595.

[25] I.E. Abdou, W.K. Pratt, Quantitative design and evaluation of enhancement/thresholding edge detectors, Proceedings of the IEEE 67 (5) (1979) 753–763.
[26] http://vismod.media.mit.edu/vismod/imagery/VisionTexture/vistex.html.
[27] http://www.eecs.berkeley.edu/Research/Projects/CS/vision/grouping/segbench/.
[28] D.R. Martin, C.C. Fowlkes, J. Malik, Learning to detect natural image boundaries using local brightness, color, and texture cues, IEEE Transactions on Pattern Analysis and Machine Intelligence (2004).
[29] P. Arbelaez, L. Cohen, Constrained image segmentation from hierarchical boundaries, CVPR (2008).
[30] J. Ning, L. Zhang, David Zhang, C. Wu, Interactive image segmentation by maximal similarity based region merging, Pattern Recognition 43 (2010) 445–456.
[31] K.H. Zhang, L. Zhang, H.H. Song, W. Zhou, Active contours with selective local or global segmentation: a new formulation and level set method, Image and Vision Computing 28 (4) (2010) 668–676.
[32] X.L. Xie, G. Beni, A validity measure for fuzzy clustering, IEEE Transactions on Pattern Analysis and Machine Intelligence 13 (1991) 841–847.